ELSEVIER

Journal of Power Sources 61 (1996) 205–211

JOURNAL OF POWER SOURCES

Catalysis of the electrochemical processes on solid oxide fuel cell cathodes

J.W. Erning, T. Hauber, U. Stimming, K. Wippermann

Institute of Energy Process Engineering (IEV), Forschungszentrum Jülich GmbH (KFA), PO Box 1913, 52425 Jülich, Germany

Abstract

Three methods of lowering the activation energy of the oxygen reduction reaction at solid oxide fuel cell (SOFC) cathodes are reported: (i) addition of highly dispersed noble metals (≤ 0.1 mg/cm^2) at the $La_{0.84}Sr_{0.16}MnO_3$ cathode/yttria stabilized zirconia (YSZ) electrolyte interface; (ii) partial substitution of manganese by cobalt in $La_{0.79}Sr_{0.16}MnO_3$ cathodes, and (iii) combination of (i) and (ii). In the presence of palladium, the apparent activation energy, E_a, of the oxygen reduction reaction is decreased from 2.2 eV ($La_{0.84}Sr_{0.16}MnO_3$ without catalyst) to 1.4 eV. A similar effect is observed, when manganese is substituted by 20 mol% Co ($La_{0.79}Sr_{0.16}Mn_{0.80}Co_{0.20}O_3$), where $E_a \approx 0.9$ eV is obtained. In the presence of palladium, with the substitution of manganese by cobalt (method (iii)), no further improvement is achieved.

Keywords: Solid oxide fuel cell; Cathodes; Catalysis

1. Introduction

An important goal in the development of solid oxide fuel cells (SOFCs) is to reduce the operating temperature of the fuel cell stack from about 1273 to below 1100 K. This goal can only be reached if electrodes with a high catalytic activity for the electrochemical reactions are developed.

In the case of the SOFC cathode, high activation energies of the oxygen reduction are obtained with standard perovskites such as $La_{0.84}Sr_{0.16}MnO_3$ (LSM) [1]. In the present paper, three methods of lowering the activation energy of the oxygen reduction reaction are reported:

(i) addition of noble metals to the common $La_{84}Sr_{16}MnO_3$ cathode;

(ii) partial substitution of manganese by cobalt in $La_{0.79}Sr_{0.16}Mn_{1-x}Co_xO_3$ cathodes, and

(iii) combination of (i) and (ii), i.e. addition of palladium to the $La_{0.79}Sr_{0.16}Mn_{0.8}Co_{0.2}O_3$ cathode.

Initial attempts with noble metal catalysts were made by impregnating the electrode particles [2]. For an optimal effect, the catalyst should be concentrated at the interface between the electrode and the electrolyte. Thus, thin layers (≈ 0.1 mg/cm^2) of highly dispersed noble metals, i.e. palladium, platinum, iridium and ruthenium, were prepared onto the yttria stabilized zirconia (YSZ8) electrolyte surface, as described in Section 5.

In previous work [3], cobalt-containing perovskites, e.g. $La_{0.80}Sr_{0.20}Mn_{0.50}Co_{0.50}O_3$, have been reported to decrease significantly the overpotential of the oxygen reduction. Nevertheless, no data concerning the apparent activation energies and pre-exponential factors of the overall reaction as a function of overpotential and cobalt content were given.

In this paper, data of the current densities of oxygen reduction and oxygen evolution on the standard perovskite (LSM84) and the modified perovskites (see methods (i)–(iii)) as a function of overpotential and temperature are reported. From the temperature dependence of the current density at different overpotentials, apparent activation energies and pre-exponential factors were calculated and plotted as a function of the overpotential. In the case of oxygen reduction, the overall reaction can be written as:

$$O_2 + 2V_O^{\cdot\cdot} + 4e^- \rightarrow 2O_O^x \quad (1)$$

In Refs. [4,5], different mechanisms for the oxygen reduction reaction have been proposed. Nevertheless, the mechanism of the oxygen reduction at the SOFC cathode is not yet clear. The following sequence of steps is one possibility to describe the reaction mechanism:

(i) diffusion of O_2 into the pores of the cathode:

$$O_2 \rightarrow O_{2,\,pore} \quad (1a)$$

(ii) adsorption of O_2 onto the cathode or catalyst surface:

$$O_{2,\,pore} \rightarrow O_{2,\,ad} \quad (1b)$$

(iii) dissociation of molecular adsorbed oxygen:

$$O_{2,\,ad} \rightarrow 2O_{ad} \quad (1c)$$

PII S0378-7753(96)02358-0

(iv) surface diffusion of atomic adsorbed oxygen to the triple contact phase (tcp):

$$O_{ad} \rightarrow O_{ad,\ tcp} \quad (1d)$$

(v) first-charge transfer:

$$O_{ad,\ tcp} + e^- \rightarrow O^-_{ad,\ tcp} \quad (1e)$$

(vi) second-charge transfer:

$$O^-_{ad,\ tcp} + e^- \rightarrow O^{2-}_{ad,\ tcp} \quad (1f)$$

(vii) oxygen-ion transfer into the electrolyte:

$$O^{2-}_{ad,\ tcp} + V_{\ddot{o}} \rightarrow O^{x}_{o} \quad (1g)$$

2. Experimental

2.1. Preparation of the cathodes

The cathode layers were prepared by screen printing using tape cast electrolyte foils as the substrates. The cathodes were made from perovskite powders which had been prepared from aqueous nitrate salt solutions (Merck, p.a.) by spray drying and had either the composition of $La_{0.84}Sr_{0.16}MnO_3$ (LSM84) or $La_{0.79}Sr_{0.16}Mn_{1-u}Co_uO_3$ with $u = 0$, 10 and 20 mol% Co on the B-site (LSM79, LSM79Co10 and LSM79Co20). A detailed description of the preparation procedure can be found in Ref. [6]. The sub-stoichiometry of the cobalt-containing perovskite on the A-site has been found to suppress the formation of insulating $SrZrO_3$ c. $La_2Zr_2O_7$ layers between YSZ8 and the perovskite [7]. The thickness of the cathode layers was ≈ 50 μm, the diameter 1 cm and the porosity about 30%. The sintering temperature was 1473 K.

2.2. Preparation of the electrolyte

The electrolyte foils consisted of 8 mol% yttria stabilized zirconia (YSZ8) with a thickness of 130 μm and a diameter of about 2 cm. They were prepared from commercial powders (Tosoh/United Ceramics) by tape casting. The electrolyte foils were sintered at 1873 K for 1 h.

2.3. Preparation of the catalyst layers

The catalyst layers were made from aqueous solutions of platinum, palladium, iridium and ruthenium salts, which were prepared using either dissolved metal pieces (Pt, 99.9%, Heraeus) or soluble salts ($PdCl_3$, $IrCl_3$, $RuCl_3$, p.a., Heraeus). The concentration of metal in the solutions was 6.25 g/l. 10 μl drops of these solutions were applied onto the YSZ8 foils. After drying, the salts were either reduced to the metal form by heating under hydrogen atmosphere at 1073 K for 1 h (Pt/Pd), or oxidized by heating under air atmosphere at 1073 K (Ir/Ru). Highly dispersed catalyst layers with a thickness of less than 0.1 mg/cm^2 were obtained. After then, the cathode layers were brought onto the prepared electrolytes, as described above.

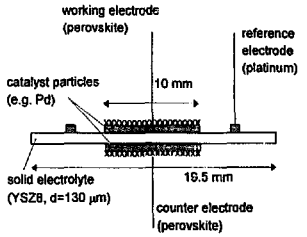

Fig. 1. Schematic view of the cross section of the measuring cell.

2.4. Cell design

A schematic picture of the cell geometry is shown in Fig. 1. The ring-shaped reference electrode was made of platinum paste (Demetron 308A). The current was supplied by using platinum nets and platinum wires. The gas compartments were separated by placing gold seals on both sides of the electrolyte.

2.5. Electrochemical apparatus

Potentiodynamic current–potential measurements were performed by means of a Schlumberger Solartron 1286 electrochemical interface. Potentiodynamic measurements were run with the 'Blue Chip Software version 2.04'. The scan rate of the potentiodynamic measurements was 1 mV/s. A correction of the current–potential curves due to ohmic losses in the electrolyte was performed by subtracting the ohmic resistance calculated from impedance spectra which were measured by using a Schlumberger Solartron 1255 frequency response analyser.

3. Results and discussion

3.1. Addition of noble metal catalysts to the LSM84 cathode

3.1.1. Current–potential measurements

First, quasi-steady-state current–potential measurements were carried out in the potential range, where oxygen reduction and oxygen evolution take place on $La_{0.84}Sr_{0.16}MnO_3$ cathodes with and without the addition of a catalyst at a temperature of 1073 K. Tafel plots, i.e. semi-logarithmic plots of the current–potential curves are shown in Fig. 2. In the presence of palladium as the catalyst, the current density increases by more than one order of magnitude as compared with samples without catalyst. With platinum as the catalyst, the current density of the oxygen reduction reaction is enhanced by nearly one order of magnitude, while the current

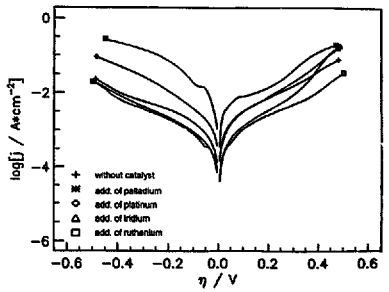

Fig. 2. Tafel plots for oxygen reduction and oxygen evolution on $La_{0.84}Sr_{0.16}MnO_3$ cathodes, comparison of cathodes without catalyst and with addition of palladium, platinum, iridium and ruthenium; data are obtained from quasi-steady-state current–potential measurements $dU/dt = 1$ mV/s, $T = 1073$ K, air atmosphere.

density of the oxygen evolution reaction is not affected within the experimental error. With the addition of iridium or ruthenium, the current density decreases in general, but especially for the oxygen evolution (as compared with values obtained in the absence of a catalyst).

In order to understand the influence of the different catalysts on the current–potential curves obtained with $La_{0.84}Sr_{0.16}MnO_3$ cathodes, it is important to distinguish their influence on the apparent activation energy and the apparent pre-exponential factor of the overall reaction. While the activation energy only reflects the electrocatalytic activity of the cathode material inclusive all catalyst layers, the pre-exponential factor correlates both the electrocatalytic activity, e.g. the number of reaction sites, and the microstructure of the electrode/electrolyte interface, e.g. the length of the reaction zone.

The apparent activation energies and the apparent pre-exponential factors of the oxygen reduction and the oxygen evolution reactions were determined from the temperature dependence of the current–potential curves obtained with the cathodes described above. The temperature range was between 1073 and 1223 K. For the example of the $La_{0.84}Sr_{0.16}MnO_3$ cathode without a catalyst, Tafel plots obtained from the current–potential curves are shown in Fig. 3. As can be seen, the increase in current density with temperature is more pronounced in the potential range of the oxygen reduction reaction. This is reflected in the Arrhenius plots (see Fig. 4) calculated for different anodic and cathodic overpotentials.

From the slope and the intercept of the Arrhenius plots at $i/T = 0$, apparent activation energies and apparent pre-exponential factors of the oxygen reduction and the oxygen evolution reactions, respectively, as a function of the overpotential were calculated, see in Fig. 5. At negative overpotentials, where the oxygen reduction is dominating, high apparent activation energies of more than 200 kJ/mol are obtained. This means, that the electrocatalytic properties of $La_{0.84}Sr_{0.16}MnO_3$ cathodes with respect to oxygen reduction, which occurs at the cathode/electrolyte interface in high temperature fuel cells, are poor. A similar result has been obtained

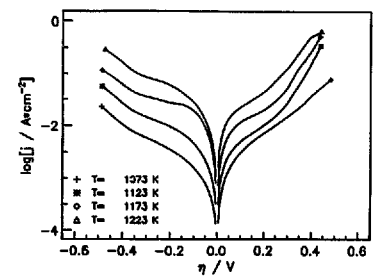

Fig. 3. Tafel plots for oxygen reduction and oxygen evolution on a $La_{0.84}Sr_{0.16}MnO_3$ cathode; $T = 1073, 1123, 1173$ and 1223 K, air atmosphere, data obtained from quasi-stationary current–potential measurements, $dU/dt = 1$ mV/s.

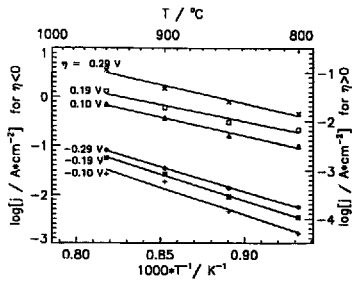

Fig. 4. Arrhenius plots calculated from current–potential curves (see Fig. 1) in the temperature range from 1073 to 1223 K, $\eta = -0.29$, -0.19, -0.1, 0.1, 0.19 and 0.29 V.

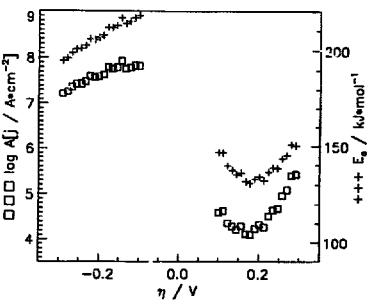

Fig. 5. $La_{0.84}Sr_{0.16}MnO_3$ cathode without catalyst; apparent activation energy, E_a, and apparent pre-exponential factor, A, as a function of overpotential, η. Values were obtained from Arrhenius plots in the potential range of -0.3 V $< \eta < 0.3$ V and the temperature range of 1073 to 1223 K (see Fig. 4).

with $La_{0.84}S_{0.16}MnO_3$ cathodes made by wet powder spraying [1]. At negative overpotentials, two potential ranges can be distinguished. At low overpotentials ($|\eta| < 200$ mV), the apparent activation energy decreases with increasing negative overpotential, while the apparent pre-exponential factor remains almost constant. This behaviour is expected for a rate-determining charge-transfer process. According to:

$$\eta < 0,\ |\eta| \gg RT/nF\ \ dE_a/d|\eta| = \alpha_c nF \quad (2a)$$

$$\eta > 0,\ \eta \gg RT/nF\ \ dE_a/d\eta = \alpha_a nF \quad (2b)$$

where α_c and α_a are the charge-transfer coefficients of reduction and oxidation reactions and n is the number of the electrons involved in the charge-transfer steps, a value of $\alpha n \approx 0.5$ is obtained from the slope of E_a–η, which is a reasonable value for a charge-transfer-controlled process. At high cathodic overpotentials ($|\eta| > 200$ mV), both E_a and $\log A$ decrease with increasing negative overpotential, which cannot be explained with a rate-determining charge-transfer step or other rate-determining steps, like surface diffusion of adsorbed oxygen species or dissociative adsorption of oxygen onto the cathode surface. In the latter case, both E_a and $\log A$ are expected to be independent of the overpotential. Thus, at high negative overpotentials, the overall reaction rate is not determined by a single partial step, but by at least two partial steps of the overall reaction. At potentials where oxygen evolution takes place, much lower apparent activation energies of about 140–150 kJ/mol are obtained. At anodic overpotentials more than 200 mV, the apparent activation energy increases with increasing overpotential. Furthermore, the apparent pre-exponential factor is strongly dependent on the overpotential and shows a similar potential dependency as compared with the apparent activation energy. These results, which have been also observed in previous experiments [1], indicate a complex reaction scheme which can only be unrevelled using additional experimental techniques.

With the addition of noble metal catalysts, the picture changes considerably. Fig. 6 shows apparent activation energies and apparent pre-exponential factors of the oxygen reduction and the oxygen evolution reactions as a function of the overpotential in the presence of palladium. In this case, the apparent activation energy of the oxygen reduction in the range of 100–140 kJ/mol is much smaller compared with the values obtained for the cathode without addition of catalyst, see Fig. 5. The effect of a decreased activation energy is partially compensated by a parallel decrease of the pre-exponential factor. A comparison of the influences of the apparent activation energy and the apparent pre-exponential factor is possible, if the values of activation energies are divided by 2.3 RT. For example at a temperature of 1073 K, a decrease of the apparent activation energy by 20.5 kJ/mol is compensated by a parallel decrease of the apparent pre-exponential factor by one order of magnitude. At a typical overpotential of -0.1 V on a high temperature fuel cell cathode, the apparent activation energy decreases from 214 kJ/mol (without catalyst, see Fig. 5) to 138 kJ/mol (addition of palladium,

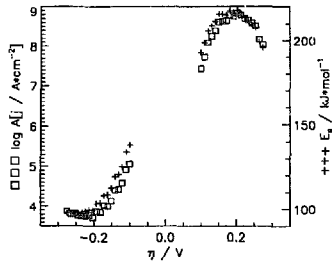

Fig. 6. $La_{0.84}Sr_{0.16}MnO_3$ cathode with the addition of palladium; apparent activation energy, E_a, and apparent pre-exponential factor, A, as a function of overpotential, η. Values were obtained from Arrhenius plots in the potential range of $-0.3\ V < \eta < 0.3$ V and the temperature range of 1073 to 1223 K.

see Fig. 6). At a temperature of 1073 K, this means a shift of $\Delta E_a/2.3RT = 3.7$. At the same overpotential, the apparent pre-exponential factor decreases from 7.8 to 5.1, which means a shift of $\Delta \log A = 2.7$. As a result, the current density increases by one order of magnitude from 1.8 mA/cm^2 (without catalyst) to 18 mA/cm^2 (addition of palladium), as shown in Fig. 2. As in the case of LSM84 without catalyst, at negative overpotentials, two potential ranges can be distinguished. In contrast to the results obtained with LSM84 without catalyst, at low overpotentials ($|\eta| < 200$ mV), both E_a and log A decrease with increasing negative overpotential, which cannot be explained with a rate-determining charge-transfer step. At high cathodic overpotentials ($|\eta| > 200$ mV), both E_a and $\log A$ are almost independent of the overpotential, which would be expected for surface diffusion or dissociation/adsorption of oxygen as rate-determining reaction steps. In the potential range of oxygen evolution, high apparent activation energies ($E_a = 190$–210 kJ/mol) and pre-exponential factors ($\log A = 8$–9) with maxima at 0.2 V are obtained. This result is surprising, since the activation energy of the oxygen evolution is strongly increased by the addition of palladium.

If platinum is present, both E_a and $\log A$ are decreased, but much less pronounced than compared with the values obtained by addition of palladium. Thus, at $\eta = -0.1$ V, the current density increases only by a factor of two. By addition of iridium or ruthenium, in the potential range of oxygen reduction, the activation energies ($E_a \approx 200$ kJ/mol) and pre-exponential factors ($\log A = 7$–8) are similar to those obtained without addition of catalysts. On the other hand, at anodic overpotentials, E_a (160–210 kJ/mol) and $\log A$ (5–8) are higher compared with values calculated for the cathode without catalyst. Again, the influence of the change of the apparent activation energy is dominating. As a result, in the presence of iridium or ruthenium, the current density of the oxygen reduction is slightly decreased, while the current density of the oxygen evolution is strongly decreased.

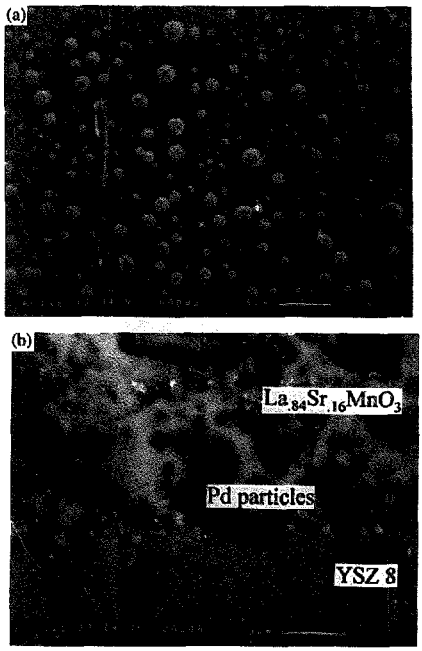

Fig. 7. (a) Scanning electron micrographs of palladium particles onto the electrolyte surface before the preparation of the cathode layer, magnification ×5000; (b) scanning electron micrographs of the cross section of the electrode/electrolyte interface after the preparation of the cathode, magnification ×6000.

3.1.2. Scanning electron micrography

Fig. 7(a) and (b) shows SEM pictures of palladium particles on the electrolyte surface before the preparation of the cathode layer (Fig. 7(a), top view) and after the preparation of the cathode (Fig. 7(b), cross section), the magnification of the micrographs is ×5000 (Fig. 7(a)) and ×6000 (Fig. 7(b)), respectively. The palladium particles were analysed by energy dispersion X-ray (EDX). As can be seen from Fig. 7(a), a distribution of the particle size of palladium in the range of <0.1 up to ≈ 1 μm is obtained. The cross section of the cathode/electrolyte interface (Fig. 7(b)) shows a similar distribution of the particle size of palladium. This means that the palladium particles do not agglomerate during the sintering process of the cathode.

3.2. Partial substitution of manganese by cobalt

Fig. 8 shows Tafel plots of oxygen reduction and oxygen evolution using $La_{0.79}Sr_{0.16}Mn_{1-u}Co_uO_3$ cathodes with $u = 0$, 10 and 20 mol% Co. With increasing amount of cobalt, the current density increases, in the case of 20% Co by one order of magnitude. From the temperature dependence of the current–potential curves, apparent activation energies and pre-exponential factors of the oxygen reduction and the oxygen evolution reactions were calculated. Table 1 shows, that with increasing cobalt content, at a cathodic overpotential of −100 mV, E_a decreases from 223 to 110 kJ/mol and log A decreases from 8.4 to 3.8. Again, the influence of the activation energy on the current density is dominating and the current density increases for 20 mol% Co as compared with 0% at 800 °C.

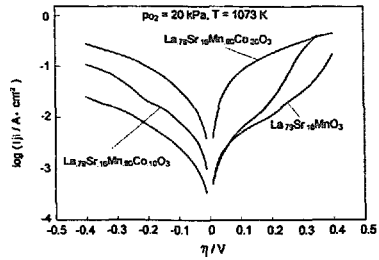

Fig. 8. Tafel plots of oxygen reduction and oxygen evolution on $La_{0.79}Sr_{0.16}Mn_{1-u}Co_uO_3$ cathodes with $u = 0$, 10 and 20 mol% Co.

For the example of the $La_{0.79}Sr_{0.16}Mn_{0.80}Co_{0.20}O_3$ cathode (LSM79Co20), the apparent activation energies and apparent pre-exponential factors as a function of the overpotential are shown in Fig. 9. At negative overpotentials, two potential

Table 1
Apparent activation energies, E_a, and apparent pre-exponential factors, log A, obtained from Arrhenius plots of the current density on $La_{0.79}Sr_{0.16}Mn_{1-u}Co_uO_3$ cathodes with $u = 0$, 10 and 20 mol% Co at an overpotential of −0.1 V and a temperature range of 1073–1223 K

Cobalt content (mol%)	E_a (kJ mol^{-1})	log A (|j|/A cm^{-2})
0	223	8.4
10	237	4.8
20	110	3.8

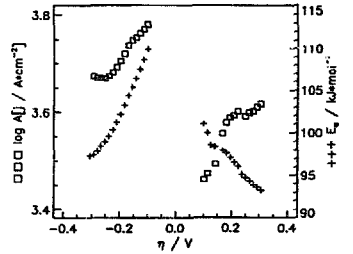

Fig. 9. $La_{0.79}Sr_{0.16}Mn_{0.8}Co_{0.2}O_3$ cathode; apparent activation energy, E_a, and apparent pre-exponential factor, A, as a function of overpotential, η. Values were obtained from Arrhenius plots in the potential range of $-0.3\ V < \eta < 0.3\ V$ and the temperature range of 1073 to 1223 K.

ranges can be distinguished. At low overpotentials ($|\eta| < 200$ mV), E_a decreases with increasing overpotential ($\alpha_c n = 0.75$, according to Eq. (2a)), while $\log A$ remains almost constant. Qualitatively, this behavior is similar to that of LSM84 without addition of a catalyst at low overpotentials and can be interpreted with a rate-determining charge-transfer process. Nevertheless, the values of E_a and $\log A$ obtained with LSM79Co20 are a factor of two smaller compared with those obtained with LSM84. At high cathodic overpotentials ($|\eta| > 200$ mV), both E_a and $\log A$ seem to be independent of the overpotential, similar to the results obtained with LSM84 + palladium at high cathodic overpotentials. Quantitatively, the values obtained with LSM79Co20 ($E_a \approx 97$ kJ/mol, $\log A \approx 3.7$) are nearly identical with those for LSM84 + palladium ($E_a \approx 100$ kJ/mol, $\log A \approx 3.8$, see Fig. 6). The latter results may be interpreted by the same rate-determining step, e.g. surface diffusion or dissociation/adsorption of oxygen, at high overpotentials on both cathodes.

In the potential range of oxygen evolution, E_a decreases with increasing overpotential ($\alpha_a n = 0.35$, according to Eq. (2b)), while $\log A$ remains almost constant, which can be interpreted with a rate-determining charge-transfer process.

3.3. Addition of palladium to the LSM79Co20 cathode

Fig. 10 shows a comparison of the catalytic activitiy of the investigated cathodes. The apparent activation energy is plotted versus the apparent pre-exponential factor for LSM84 and LSM79Co20 cathodes with and without the addition of palladium. The data were obtained from the temperature dependency of the current density at an overvoltage of -100 mV, which is a typical overvoltage at the SOFC cathode under practical conditions. Since the overall current density at a constant overpotential can be written as:

$$\log j = \log A - (E_a / 2.3RT) \qquad (3)$$

straight lines corresponding to constant-current densities are obtained in the E_a–$\log A$ plot for a constant temperature. The four lines indicated in Fig. 10 correspond to four current densities in the range of 1 mA/cm² to 1 A/cm² and are calculated for a temperature of 1073 K. As can be seen from Fig. 10, the same E_a and $\log A$ values are obtained for LSM79Co20 and LSM84 with the addition of palladium, although the E_a and $\log A$ values for the same cathodes without the addition of a catalyst differ significantly. Thus, almost the same current density of about -30 mA/cm² at $T = 1073$ K and $\eta = -0.1$ V is obtained for the modified cathodes shown in Fig. 10. This means, that a combination of method (i) (addition of noble metal catalyst) and method (ii) (partial substitution of manganese by cobalt) yields no further improvement in electrocatalytic activity of the cathode as compared with either method (i) or method (ii). The results suggest, that in the pre nce of palladium, the oxygen reduction predominantly takes place in the palladium layer. Thus, the overall rate of oxygen reduction is determined by palladium, independent of the composition of the perovskite cathode. Moreover, this means that the rate-determining partial reaction step(s) occur(s) within a distance from the cathode/electrolyte interface, which is equal to or smaller than the thickness of the palladium layer, i.e. ≤ 1 μm.

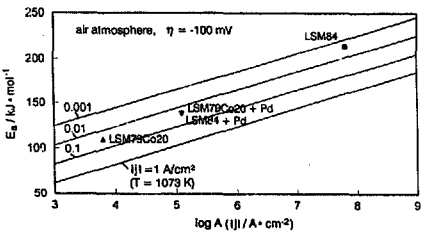

Fig. 10. Apparent activation energies, E_a, vs. apparent pre-exponential factors, $\log A$, obtained from Arrhenius plots at an overpotential of -0.1 V and a temperature range of 1073 to 1223 K. Values for (■) LSM84, (▲) LSM79Co20, (▼) LSM84 + Pd, and (●) LSM79Co20 + Pd. Straight lines indicate different current densities (0.001, 0.01, 0.1 and 1 A/cm²).

4. Conclusions

As shown above, the high apparent activation energy (≈ 200 kJ/mol) of oxygen reduction on $La_{0.84}Sr_{0.16}MnO_3$ is strongly decreased ($E_a \approx 100$ kJ/mol) by the addition of small amounts of highly dispersed palladium (≤ 0.1 mg/cm²) (method (i)) or by substitution of manganese by 20 mol% Co on the B sites of the perovskite cathode (method (ii)). The apparent pre-exponential factor, A, also decreases, but to a lesser extent. As a result, the current density of oxygen reduction increases by more than one order of magnitude, if palladium is added or manganese substituted by 20 mol% Co.

With the addition of platinum, the current density of oxygen reduction still increases by a factor of two, whereas in the case of addition of ruthenium or iridium, no improvement in electrocatalytic activity of the $La_{0.84}Sr_{0.16}MnO_3$ cathode is obtained.

The addition of palladium to the $La_{0.79}Sr_{0.16}Mn_{0.80}Co_{0.20}O_3$ cathode (method (iii)) yields at low cathodic overpotential ($\eta = -0.1$ V) the same apparent activation energy and pre-exponential factor as obtained with $La_{0.84}Sr_{0.16}MnO_3$ + palladium. This can be explained by an oxygen reduction reaction which mainly takes place within a thin palladium catalyst layer ≤ 1 μm.

From the dependence of the apparent activation energy and the pre-exponential factor on the overpotential, it follows, that at low cathodic overpotentials ($|\eta| < 200$ mV), the slopes of $dE_a/d\eta$ and $d \log A/d\eta$ obtained with $La_{0.84}Sr_{0.16}MnO_3$ can be explained by a rate-determining charge-transfer step. This means that at low cathodic overpotentials the improvement of the electrocatalytic activity of

the $La_{0.84}Sr_{0.16}MnO_3$ cathode by the modification methods described above is mainly due to the catalysis of the charge-transfer reaction(s). At high cathodic overpotentials, surface diffusion of adsorbed oxygen species or adsorption and dissociation of oxygen molecules may play an important role.

Acknowledgements

The authors gratefully acknowledge the fruitful discussions with Mr H. Kabs and the screen printing of the cathodes by Dr W. Schaffrath (Fraunhofer-Einrichtung für keramische Technologien und Sinterwerkstoffe, 01277 Dresden).

References

[1] J. Divisek, L.G.J. de Haart, P. Holtappels, T. Lennartz, W. Malléner, U. Stimming and K. Wippermann, *J. Power Sources, 49* (1994) 257.
[2] M. Watanabe, H. Uchida, M. Shibata, N. Mochizuki and K. Amikura, *J. Electrochem. Soc., 141* (1994) 342.
[3] E. Ivers-Tiffée, M. Schiessl, H.J. Oel and W. Wersing, in F.W. Poulsen, J.J. Bentzen, F. Jacobsen, E. Shou and M.J.L. Østergård (eds.), *Proc. 14th Risø Int. Symp. Materials Science, Roskilde, Denmark, 1993*, p. 69.
[4] B.A. van Hassel, B.A. Boukamp and A.J. Burggraaf, *Solid State Ionics, 48* (1991) 155.
[5] M.J.L. Ostergard and M. Mogensen, *Electrochim. Acta, 38* (1993) 2015.
[6] E. Syskakis, W. Jungen and A. Naoumidis, in F. Aldinger (ed.), *Proc. Int. Conf. Materials, Dresden, Germany, 1993*, p. 707.
[7] G. Stochniol, E. Syskakis and A. Naoumidis, in P. Biedermann and B. Krahl-Urban (eds.), *Proc. 5th IEA Workshop, Jülich, Germany, 1993*, p. 25.